Prostaglandin E_1 Abrogates Early Reductive Stress and Zone-specific Paradoxical Oxidative Injury in Hypoperfused Rat Liver

Hidekazu Suzuki, Makoto Suematsu,* Hiromasa Ishii, Shinzo Kato, Hideho Miki,* Mikiji Mori, Yuzuru Ishimura,* Takeshi Nishino,‡ and Masaharu Tsuchiya

**Departments of Internal Medicine and Biochemistry, School of Medicine, Keio University, Tokyo 160, Japan; and ‡Department of Biochemistry and Molecular Biology, Nippon Medical University, Tokyo 113, Japan*

Abstract

This study was designed to investigate the effects of prostaglandin E_1 on reductive stress and the subsequent oxidative cell injury in hypoperfused rat liver. The intralobular heterogeneity of hepatocellular redox state, mitochondrial dysfunction, and intracellular hydroperoxide formation were visually monitored by digital microfluorography of pyridine nucleotide autofluorescence, rhodamine 123, and dichlorofluorescein fluorescence, respectively. Under the 25% low flow perfusion, pyridine nucleotide autofluorescence increased time-dependently and reached a steady state at 10 min among the entire lobules. The decrease in mitochondrial membrane potential was > 20 mV in all portions of the lobules at 60 min. The onset of hydroperoxide formation was observed at 40 min in the marginally oxygenated proximal portion of anoxic pericentral regions and the oxidative impact reached a maximum level at 60 min. Sodium (−)-8-(3-methoxy-4-phenylsulfinylphenyl) pyrazo [1,5-a]-1,3,5-triazine-4-olate monohydrate (BOF 4272), a novel xanthine oxidase inhibitor, suppressed the zone-specific oxidative changes without attenuating the increase in pyridine nucleotide autofluorescence and mitochondrial dysfunction. Pretreatment with prostaglandin E_1 not only abrogated an early increase in pyridine nucleotide fluorescence and mitochondrial dysfunction induced by hypoperfusion but also diminished the subsequent midzonal oxidative injury. Since prostaglandin E_1 has no oxyradical-scavenging action, the preventive effect of this reagent on the hypoxia-induced oxidative cell injury is attributable to the attenuation of mitochondrial dysfunction. These results suggest that, in low flow hypoxia, early reductive stress plays a key role in the initiation of xanthine oxidase–mediated midzonal oxidative changes, which may lead to subsequent centrilobular necrosis. (*J. Clin. Invest.* 1994. 93:155–164.) Key words: hypoxia • xanthine oxidase • oxygen radicals • nicotinamide adenine dinucleotide reduced form • redox state

Introduction

Hypoxic liver injury is of major clinical importance in hemorrhagic shock, endotoxemia, metabolic disorders induced by ethanol administration (1, 2), and primary nonfunction in liver transplantation (3). There is a body of evidence showing that mitochondrial damage due to impaired oxygen supply is important as a mechanism of irreversible liver injury. Lemasters et al. (1), who examined isolated rat hepatocytes exposed to anoxia-mimicking reagents, has stated that a decrease in mitochondrial inner membrane potential may play a crucial role in bleb formation and subsequent cell death. When the liver is exposed to the prolonged impairment of sinusoidal blood supply, the mitochondrial function of hepatocytes in anoxic pericentral regions should be more easily impaired than in relatively well-oxygenated periportal regions. Accordingly, during low flow hypoxia in which an intralobular gradient of oxygen supply is observed, hepatocytes in the most distal portion of microcirculatory units are expected to show a loss of viability followed by the extension of the damage towards the proximal portion of the lobule.

However, the actual time course of the intralobular distribution of cell injury during hypoxia seems quite different. According to Marotto et al. (4), low flow hypoxia-induced cell injury occurs first in the intermediate zone between the periportal and pericentral regions and extends towards the distal portion of hepatic microcirculatory units, producing centrilobular necrosis. Furthermore, our recent observation has revealed that, even under hypoxic condition, the oxidative stress occurs paradoxically in the midzonal region rather than in the anoxic pericentral regions (5). Because of these findings, the relationship between mitochondrial dysfunction and oxygen radical formation in hypoxic liver injury remains unclear.

The aim of this study is to investigate the mechanism by which hypoxia-induced mitochondrial dysfunction evokes oxidative cell injury during 25% low flow hypoxia. To that effect, we used dual-color digital microfluorography using two different functional fluorescence probes, rhodamine 123 (Rh123)[1] and propidium iodide (PI), which revealed spatial and temporal alterations of mitochondrial function and cell death simultaneously in a hepatic microcirculatory unit (1, 6). Furthermore, the temporal and spatial alterations of intrahepatic

Preliminary reports of this work were presented at the annual meeting of the American Association for the Study of Liver Diseases, Chicago, IL, 3 November 1992.

Address correspondence to Dr. Masaharu Tsuchiya, Department of Internal Medicine, School of Medicine, Keio University, 35 Shinanomachi, Shinjuku-ku, Tokyo 160, Japan.

Received for publication 10 February 1993 and in revised form 9 August 1993.

J. Clin. Invest.

0021-9738/94/01/0155/10 $2.00
Volume 93, January 1994, 155–164

1. *Abbreviations used in this paper:* BOF4249, 8-[4-(4-bromophenylthio)-3-methylphenyl]-4-hydropyrazolo [1,5-a]-1,3,5-triazine; BOF4272, sodium (−)-8-(3-methoxy-4-phenylsulfinylphenyl)pyrazo [1,5-a]-1,3,5-triazine-4-olate monohydrate; DCF, dichlorofluorescein; DCFH, dichlorofluorescein; LDH, lactate dehydrogenase; LF, low flow; MCLA, 2-methyl-6-(*P*-methoxy-phenyl-3,7-dihydroimidazo [1,2-a] pyrazin-3-one [methyl cypridina luciferin analogue]); PI, propidium iodide; PN, pyridine nucleotide; Rh123, rhodamine 123.

pyridine nucleotide (NAD[P]H) autofluorescence during hypoxia were investigated as a marker of reductive stress (7, 8). We also investigated microtopography of oxidative changes in the hypoperfused liver using a hydroperoxide-sensitive fluorochrome, dichlorofluorescein (DCFH) diacetate (5, 9–11). Among these functional parameters, our study showed that panlobular elevation of pyridine nucleotide fluorescence is a significant phenomenon that occurs in the earliest period of hypoxia. We have demonstrated a distinct effect of PGE_1 on hypoxia-induced oxidative cell injury via its preventive action on mitochondrial dysfunction, i.e., PGE_1 significantly attenuated early panlobular reductive stress, depression of mitochondrial membrane potential, and subsequent midzonal oxidative injury during the 25% low flow hypoxia. Since PGE_1 per se has no oxyradical-scavenging action, the preventive effect of this reagent on hypoxia-induced oxidative cell injury seems to be a consequence of attenuation of mitochondrial dysfunction, which may diminish ATP degradation and subsequent xanthine oxidase–mediated oxidant formation in incompletely oxygenated midzonal regions.

Methods

Animal preparation. Male Wistar rats (200–240 g) allowed free access to laboratory chow and tap water were fasted 24 h before experiments. After the animals were anesthetized with pentobarbital sodium (30 mg/kg intraperitoneally), the livers were perfused with hemoglobin- and albumin-free Krebs-Henseleit bicarbonate-buffered solution (pH 7.4, 37°C) gassed with carbogen (95% O_2, 5% CO_2) as described previously (5, 6). The perfusate was pumped through the liver with a peristaltic pump at a constant flow rate (3.0 ml/min per g liver wt) in a single pass mode. Low flow hypoxia was performed by reducing the perfusion rate at 25% of the control flow rate (5, 6).

Dual-color microfluorography using rhodamine 123 and propidium iodide. Rh123 is a fluorescent dye that accumulates electrophoretically in the mitochondria of viable cells in response to a potential difference ($\Delta\Psi$) across the mitochondrial membrane (1, 12). Namely, Rh123 was dissolved in the perfusate to yield a final concentration of 0.8 μM, which is low enough to maintain the mitochondrial viability of hepatocytes (12). The isolated liver was perfused with the Rh123-containing Krebs-Henseleit solution by transportal infusion for 10 min. The Rh123 remaining in the intravascular space was washed out by perfusing an Rh123-free perfusate for 10 min. Then, PI was added to the perfusate to give a final concentration of 1.0 μM to assess cell viability (5, 6, 9, 11). Under epiillumination at 480 nm, Rh123-associated fluorescence was passed through a 520-nm band pass filter (BA 520; Nikon, Tokyo, Japan). PI-associated fluorescence was visualized by epiilluminating at 535 nm with passage through a 590-nm band pass filter (BA 590; Nikon). By changing the filter combination, both PI- and Rh123-derived hepatic fluorographs were alternately visualized using a silicon-intensified target camera (C-2400-08; Hamamatsu Photonics, Hamamatsu, Japan) and a quartz objective lens (at a magnification of 10). These fluorographs were digitally processed and analyzed with a computer-assisted image processor (ARGUS 200; Hamamatsu Photonics, Hamamatsu, Japan) (5, 6, 13, 14).

Data analysis of Rh123- and PI-fluorographs. After the PI- and Rh123-fluorographs were taken, a 2.0% solution of FITC-BSA was injected into the perfusion circuit at a rate of 100 μl/s for 3 s to facilitate recognition of the topography of the hepatic microangioarchitecture and the state of perfusion in the individual lobules under observation. The time course of the fluorescence tracer was recorded into a digital videorecorder (S-VHS-HQ; Victor-JVC, Tokyo, Japan). The lobular landmarks, terminal portal venules (P) and central venules (C), were identified using our previous methods described elsewhere (5, 6). To investigate the spatial and temporal alterations of cell death during low flow hypoxia, the net increase in PI-associated fluorescence was calculated by subtracting the control image (time 0) from each fluorograph recorded after the onset of the low flow procedure according to the following equation:

$$\Delta I_{PI}(x, y, t) = I_{PI}(x, y, t) - I_{PI}(x, y, 0)\ (\text{count/pixel}),$$

where (x, y) is the position of a pixel in the video frames; $I_{PI}(x, y, t)$ is the fluorescence intensity at pixel (x, y) at time t in PI-associated hepatic fluorographs; $I_{PI}(x,y,0)$ is the intensity at pixel (x, y) before starting low flow perfusion; and $\Delta I_{PI}(x, y, t)$ expresses the net increase in fluorescence during low flow hypoxia at pixel (x, y) at time t.

The temporal changes in mitochondrial membrane potential in the hepatic lobules were investigated by estimating relative Rh123 fluorescence intensity [%Rh123 (x, y, t)] according to our previous method (6). Using the digitally composed images [$\Delta I_{PI}(x, y, t)$ and %Rh123 (x, y, t)], intrahepatic Rh123- or PI-derived fluorescence was estimated at the respective measurement sites, which were restricted by variable-frame circular diaphragms containing 100 pixels. Since nonfluorescent vascular spaces were found in Rh123-associated fluorographs, %Rh123 (x, y, t) was expressed as the mean value at over 20 pixels which were located in parenchymal areas inside each circular diaphragm. Two or three different lobules that were located in the centers of microscopic fields were chosen from each experiment to avoid a possible optical error due to a marginal shading effect. Since the mitochondrial inner membrane potential ($\Delta\Psi$) is proportional to the logarithmic values of the intensity of Rh123 fluorescence in hepatocytes, the net depletion of the membrane potential ($d\Delta\Psi$) during hypoxia could be estimated according to the following equation, as described elsewhere (6):

$$\begin{aligned} d\Delta\Psi(x, y, t) &= \Delta\Psi(x, y, t) - \Delta\Psi(x, y, 0) \\ &= K \log [I_{RH}(x, y, t) - I_{BG}(x, y)] \\ &\quad - K \log [I_{RH}(x, y, 0) - I_{BG}(x, y)] \\ &= K \log [I_{RH}(x, y, t) - I_{BG}(x, y)/I_{RH}(x, y, 0) - I_{BG}(x, y)] \\ &= K \log [\%\ \text{Rh123}(x, y, t)]\ (\text{mV}), \end{aligned}$$

where K is the constant obtained using the Nernst equation and assumed to be 59 (mV), according to the methods described by Lemasters et al. (1, 6, 15). In another set of experiments, the outlet perfusate was sampled at the end of experiments (120 min after the start of hypoperfusion) and stored at −80°C to determine the activity of lactate dehydrogenase (LDH) according to the previous method (16).

Microfluorography for intralobular pyridine nucleotide autofluorescence. In a separate group, spatial and temporal alterations in intralobular pyridine nucleotide (PN) autofluorescence were visually investigated during low flow hypoxia using the same system. Although PN autofluorescence has been measured to assess the redox state in various organs, it has recently been shown that vitamin A autofluorescence in fat-storing Ito cells disturbs hepatic PN evaluation by ultraviolet-elicited spectrophotometry (7). We therefore performed digital microfluorography of intrahepatic PN autofluorescence after vitamin A autofluorescence had been abolished by a short period of ultraviolet epiillumination, as described elsewhere (8). Briefly, the surface of the perfused liver was exposed to the ultraviolet epiillumination at 360 nm for 30 s, during which vitamin A–associated autofluorescence in Ito cells was eliminated. To confirm recovery from minimal PN photobleaching, the preparation was kept under light-free conditions for 10 min. During this period, intrahepatic PN levels established a steady state (data not shown) (8, 17). The preparation was epiilluminated at 360 nm and the fluorescence at 450 nm was visualized by the silicon-intensified target camera assisted by the aforementioned computer-assisted image processor. To evaluate the spatial distribution and temporal alterations of intrahepatic PN autofluorescence during low flow hypoxia, each PN fluorograph was digitally processed and the marginal shading effect due to inhomogeneity of the camera sensitivity was corrected as described below. Namely, a fluorescent image of NADH solution at 1.0 μM [I_{NADH}-sol (x, y)] was recorded under the same

setup for the camera sensitivity at the end of each experiment. Fluorescence intensity at time t at pixel (x, y) in the microscopic field [$\%I_{NAD(P)H}(x, y, t)$] was expressed as a relative intensity versus the initial periportal PN intensity before starting low flow hypoxia [$I_{NAD(P)h}(X_P, Y_P, 0)$], as follows:

$$\% I_{NAD(P)H}(x, y, t) = \frac{I_{NAD(P)H}(x, y, t)/I_{NADH\text{-}sol}(x, y)}{I_{NAD(P)H}(X_P, Y_P, 0)/I_{NADH\text{-}sol}(X_P, Y_P)} \times 100\,(\%),$$

After completing the observation period for PN autofluorography (20 min), a 2.0% solution of FITC-BSA was injected to the perfusate circuit at a rate of 100 μl/s for 3 s and the dynamics of sinusoidal perfusion were videotaped to facilitate recognition of the topography of the hepatic microangioarchitecture. To determine whether PGE_1 administration may influence local perfusion during the low flow hypoxia, the difference of in situ sinusoidal flow was evaluated in the livers treated with and without the reagent. The replayed video images showing FITC-BSA hepatic microangiography were then introduced into an offline videodensitometer (Capiflow; IM-Capiflow, Kista, Sweden), which allowed us to show the temporal profile analysis of the changes in fluorescence at desired portions of the hepatic lobules under observation (5). Briefly, temporal profiles of the intensity of FITC-BSA fluorescence were traced in periportal regions (P) as well as in the distal pericentral regions adjacent to central venules (C) using two square video windows ($50 \times 50\ \mu m^2$). Time when the peak fluorescence intensity was obtained in each portion was automatically recorded after the dye injection. Since there is a delay of time at the peak fluorescence intensity in the pericentral region, the velocity of sinusoidal FITC-BSA movement in the individual lobules ($V_{P\text{-}C}$) can be measured as follows:

$$V_{P\text{-}C} = L_{P\text{-}C}/\Delta T_{P\text{-}C}\,(\mu m/s),$$

where $L_{P\text{-}C}$ is the distance between the centers of the measurement windows in periportal and pericentral regions, and $\Delta T_{P\text{-}C}$ is the time delay of the peak intensity in the periportal and pericentral regions. By changing the position of these windows to different venules, three to four measurements were able to be carried out in a single experiment. Such measurements were repeated using livers taken from six animals (low flow [LF] alone and PGE_1 plus LF, $n = 3$ for each group). The correlation between the individual values of $V_{P\text{-}C}$ and those of $\%\ I_{NAD(P)H}$ in the same pericentral regions at 20 min after the start of low flow perfusion was evaluated between the groups pretreated with and without PGE_1.

DCFH diacetate-dependent microfluorography. In a separate set of experiments, DCFH diacetate–dependent microfluorography was applied to the isolated perfused liver to visualize intracellular oxidative events in hepatic microcirculatory units during the 25% low flow hypoxia. DCFH diacetate and dichlorofluorescein (DCF) were purchased from Molecular Probes, Inc. (Eugene, OR) and were dissolved in absolute ethanol at a concentration of 5.0 mM. The isolated liver was perfused with DCFH diacetate–containing Krebs solution for 10 min via a transportal infusion at a final concentration of 5.0 μM. DCFH diacetate in the intravascular space was washed out with the DCFH diacetate–free perfusate for 20 min. Low flow hypoxia was performed by reducing the perfusion rate to 25% of the aforementioned control flow rate for 100 min. Temporal changes in intracellular hydroperoxide formation in the liver were investigated by estimating the apparent DCF fluorescence intensity [$\%I_{DCF}(x, y, t)$] according to the following equation:

$$\%I_{DCF}(x, y, t) = \frac{I_{DCF}(x, y, t) - I_{BG}(x, y)}{I_{DCF}(X_P, Y_P, 0) - I_{BG}(X_P, Y_P)} \times 100\,(\%),$$

where $I_{DCF}(x, y, t)$ is the rare fluorescence intensity at pixel (x, y) at time t in the DCF fluorographs; $I_{BG}(x, y)$ is the background intensity at pixel (x, y) measured before pretreatment with DCFH diacetate; (X_P, Y_P) is the site of measurement corresponding to the periportal region in each hepatic lobule; and $I_{DCF}(X_P, Y_P, 0)$ is the intensity of DCF fluorescence at (X_P, Y_P) before starting the low flow perfusion (5). The values of $\%I_{DCF}(x, y, t)$ and $\%I_{NAD(P)H}(x, y, t)$ in five different portions of the lobule were determined using a variable digital diaphragm according to the method used for Rh123 and PI fluorography.

Interventions. Effects of PGE_1 on hypoxia-induced alterations in mitochondrial function, oxidative metabolism, and cell viability were evaluated in the perfused liver using the digital microfluorography described above. PGE_1 (Ono Pharmaceutical Co., Ltd., Osaka, Japan) was added into the perfusate to give a final concentration of 100 μg/liter, 20 min before the 25% low flow perfusion. BOF4272 (sodium [−]-8-(3-methoxy-4-phenylsulfinylphenyl) pyrazo[1,5-a]-1,3,5-triazine-4-olate monohydrate), a de novo synthetic xanthine oxidase inhibitor, and BOF4249 (8-[4-(4-bromophenylthio)-3-methylphenyl]-

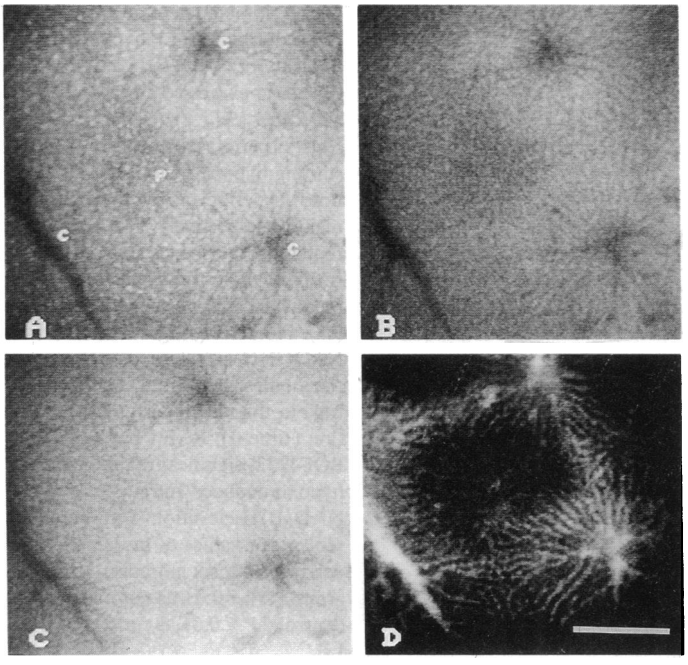

Figure 1. A representative picture of ultraviolet-elicited autofluorographs of the perfused liver microcirculation and the effects of 25% low flow hypoxia. The peak epiilluminating wave length is 360 nm. (A) A microfluorograph before the start of a continuous ultraviolet epiillumination (30 s). Note that diffuse parenchymal autofluorescence is overlaid with multiple patchy fluorescence activities derived from vitamin A in Ito cells. (B) The microfluorograph in the same microscopic field after completing the continuous ultraviolet epiillumination followed by the 10-min illumination-free period. Intralobular gradient of pyridine nucleotide autofluorescence was featured after eliminating Ito cell autofluorescence. (C) Effects of 25% low flow hypoxia for 20 min on pyridine nucleotide autofluorescene. Both periportal and pericentral regions show a rapid increase in the fluorescence intensity. (D) Hepatic microangiograph recorded after injecting FITC-BSA from the portal inlet. P and C denote portal and central venules, respectively. Bar represents 200 μm.

4-hydroxypyrazolo [1,5-a]-1,3,5-triazine) were gifts from Otsuka Pharmaceutical Factory, Inc., (Naruto, Japan). Although the chemical structure of BOF4272 is similar to that of BOF4249, the K_i values of BOF4272 and BOF4249 for xanthine oxidase were ranged at the order of 10^{-9} M and 10^{-5} M, respectively (18). To confirm the specific inhibitory effects of BOF4272 on xanthine oxidase–mediated oxidative changes in hypoperfused liver, either of these reagents was added to the perfusate at a final concentration of 10 nM, 20 min before the start of 25% low flow hypoxia in a separate set of experiments.

To check the nonspecific free radical–scavenging properties of PGE_1, BOF4272, and BOF4249, the in vitro effects of these reagents on xanthine oxidase–dependent superoxide production were assessed by a chemiluminescence method using a luciferin analogue, 2-methyl-6-(*P*-methoxy-phenyl-3,7-dihydroimidazo [1,2-a] pyrazin-3-one [methyl cypridina luciferin analogue]) (MCLA) (19, 20). The mixture containing 50 μM hypoxanthine, 6.7×10^{-5} U/ml xanthine oxidase (Sigma Chemical Co., St. Louis, MO), and 6.0 μM MCLA was prepared for the in vitro source of superoxide generation. After checking the basal chemiluminescence activity, the reaction was initiated by adding hypoxanthine to the system. MCLA-dependent chemiluminescence activity was determined using a multichannel luminometer (Biolumat 9505; Berthold GmbH, Bad Wildbad, Germany). Actual chemiluminescence activity was estimated as the difference between the maximum and basal chemiluminescence counts. Chemiluminescence activities were also determined in the presence of PGE_1 (100 μg/liter) or BOF4272 or BOF4249 (10 nM) and were expressed by the percentage activities versus the controls. In separate experiments, the effects of these reagents on MCLA-dependent photoemission derived from isolated neutrophils were also investigated. Neutrophils were isolated from peripheral blood samples taken from healthy human subjects (13), and suspensions were prepared using Eagle's MEM solution at 1×10^6 cells/ml. In the presence of MCLA (6.0 μM), chemilumines-

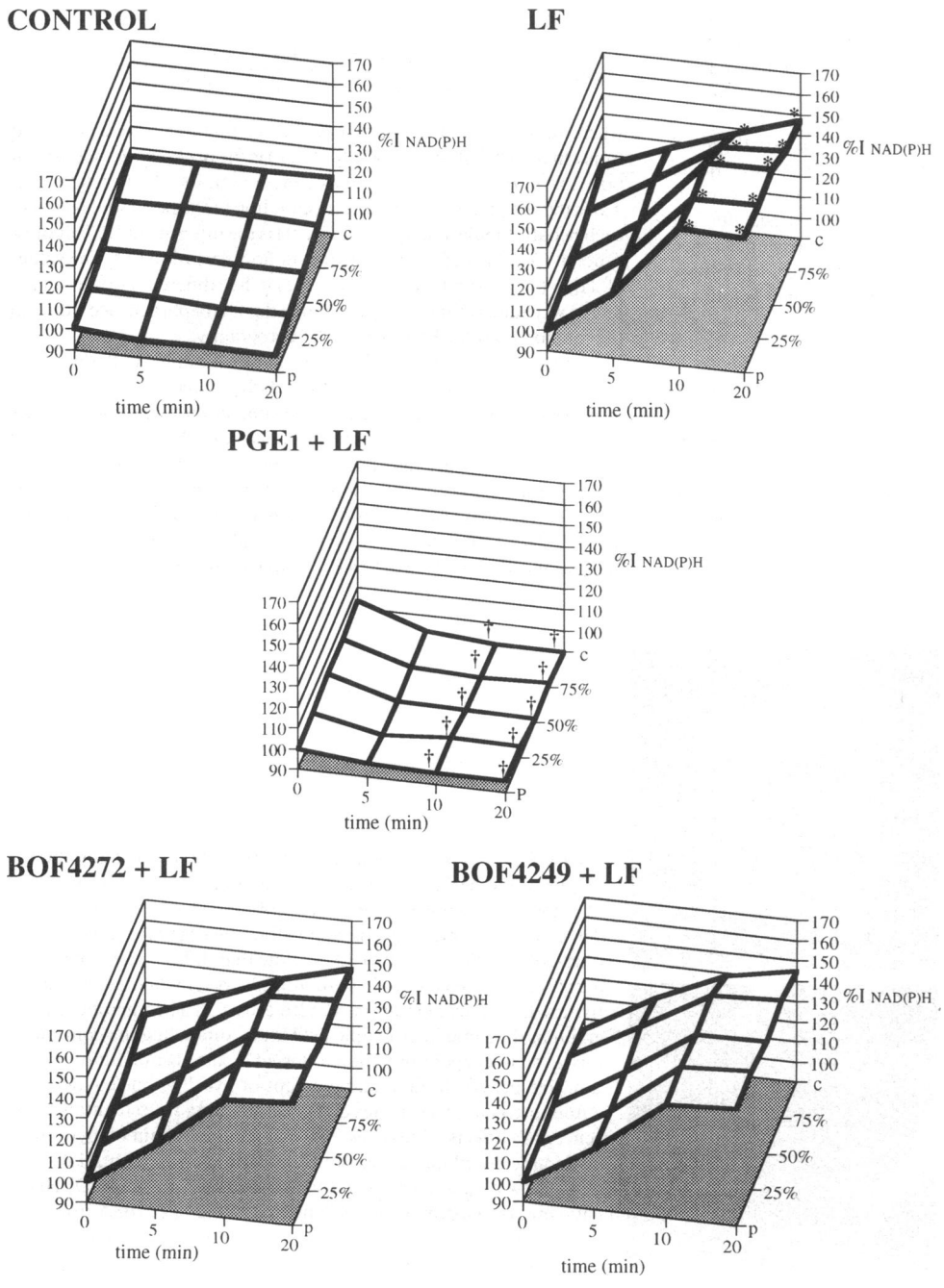

Figure 2. Topographic distribution and temporal alteration of intralobular pyridine nucleotide autofluorescence during 25% LF hypoxia. The intensity of NAD(P)H autofluorescence was expressed as the percentage values [$\%I_{NAD(P)H}$] versus controls in periportal regions before starting hypoperfusion. P and C denote the periportal and pericentral regions, respectively. The axis P–C represents the percentage distance from the periportal region regarding the distance between P and C as 100 (%). Note a slight gradient of NAD(P)H autofluorescence among the lobules (periportal < pericentral) in the normoperfused condition (time 0). PGE_1, but not BOF4272, significantly attenuated hypoxia-induced intrahepatic NAD(P)H elevation. Data represent mean values of measurements derived from six animals in each group. $^*P < 0.01$ as compared with control. $^\dagger P < 0.01$ as compared with LF.

cence activities were evoked by adding phorbol myristate acetate to a final concentration of 0.1 μg/ml. The maximum chemiluminescence activities were monitored using the aforementioned luminometer and compared among groups with and without reagents (21).

Experimental groups and statistical analysis. 30 animals were used for each experimental group using different fluorogenic probes (rhodamine 123/propidium iodide, dichlorofluorescin diacetate, and PN autofluorescence). These animals were divided into five subgroups (control, LF, PGE_1 plus LF, BOF4272 plus LF, and BOF4249 plus LF; $n = 6$ for each). 18 animals were used for the LDH assay in the perfusate sampled from hypoperfused livers (control, LF, PGE_1 plus LF; $n = 6$ for each). Differences of the data among the groups were analyzed by two-way ANOVA combined with Scheffe-type multiple comparison test. A value of $P < 0.01$ was considered significant.

Results

PGE_1 attenuates early reductive stress in hypoperfused liver. Fig. 1 illustrates spatial and temporal alterations in PN autofluorescence during the 25% low flow hypoxia. As reported previously (7), ultraviolet epiillumination evoked not only diffuse parenchymal autofluorescence (NAD[P]H) but also multiple patchy autofluorescence in perisinusoidal regions which is derived from vitamin A in Ito cells. After the liver was exposed to a continuous ultraviolet epiillumination for 30 s, a majority of vitamin A autofluorescence was eliminated because of its rapid photobleaching property (7, 8). While diffuse parenchymal autofluorescence also decreased slightly (< 10% of control), the fluorescence intensity showed a rapid recovery and reached a plateau level within 10 min after completing the epiillumination for vitamin A photobleaching (Fig. 1 *B*). Under normoperfusion, NAD(P)H autofluorescence in pericentral regions was slightly higher than in periportal regions, showing an intralobular gradient. Fig. 2 shows semiquantitative patterns of intrahepatic PN autofluorescence during the low flow hypoxia. The NAD(P)H level in the pericentral region was always higher than that in the periportal region, showing an intralobular gradient of the autofluorescence. After starting hypoperfusion, PN autofluorescence underwent a rapid increase throughout lobules and the initial gradient of NAD(P)H elevation was steeper in periportal regions than in pericentral regions. Within 10 min of the hypoperfusion period, intrahepatic NAD(P)H intensity reached a plateau and the intralobular gradient of fluorescence was eliminated (Fig. 1 *C*). Pretreatment with PGE_1, but not BOF4272 or BOF4249, significantly attenuated hypoperfusion-induced early NADH elevation in any portion of hepatic lobules. To clarify the possibility that PGE_1 might modulate intrahepatic oxygen demand by increasing sinusoidal perfusion, intralobular dynamics of transportally injected FITC-BSA were evaluated by a videodensitometer. Fig. 3 illustrates the relationship between the sinusoidal perfusion velocity ($V_{P\text{-}C}$) and PN autofluorescence at 20 min after the start of hypoperfusion [$\%I_{NAD(P)H}$ ($t = 20$)]. These results suggest that PGE_1 may abolish early reductive stress in hypoperfused liver without modifying the dynamics of sinusoidal perfusion.

PGE_1 attenuates hypoxia-induced mitochondrial dysfunction. As we previously reported in relation to the spatial distribution and temporal changes of Rh123 fluorescence in the normoperfused liver (6), Rh123 stained the entire hepatic lobule but the area close to the portal venules was preferentially labeled. Throughout the entire course of observation (100 min), there was no significant depletion of Rh123 fluorescence at any

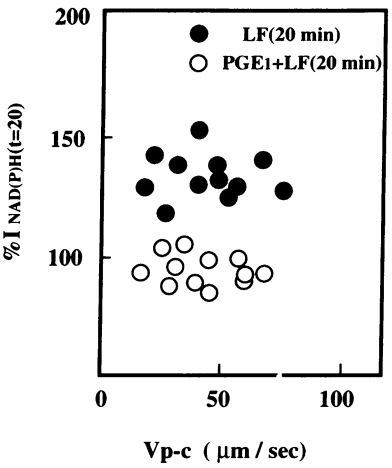

Figure 3. The relationship between sinusoidal perfusion velocity ($V_{P\text{-}C}$) and the intensity of pyridine nucleotide autofluorescence at 20 min after the start of LF hypoxia [$\%I_{NAD(P)H}$ ($t = 20$)], and effects of PGE_1 pretreatment. Open and closed circles denote the data in the groups treated with and without PGE_1, respectively. Note that PGE_1 pretreatment attenuates the hypoperfusion-induced increase in pyridine nucleotide autofluorescence without modifying the state of sinusoidal perfusion in situ. 12 data measured in 12 different lobules of three livers are represented.

sites measured, showing that mitochondrial function was well maintained in the normoperfused liver (6). Fig. 4 illustrates spatial and temporal alterations in net depletion of mitochondrial membrane potential ($d\Delta\Psi$) among groups. In low flow hypoxia, a significant $\Delta\Psi$ decrease was observed in pericentral regions at 20 min (regions expressed by 75% and *C* in plots of Fig. 4). The $\Delta\Psi$ values decreased significantly in the entire lobules at 40 min and the actual $\Delta\Psi$ decrease reached > 20 mV in all portions of the lobules at 60 min. When hypoxia was prolonged to 100 min there was a large $\Delta\Psi$ fall, especially in the pericentral regions. PGE_1 treatment significantly prevented the hypoxia-induced depletion of mitochondrial membrane potential at all measurement sites during the entire course of observation. However, neither BOF4272, a specific xanthine oxidase inhibitor, nor BOF4249 displayed any significant inhibitory effect on the $\Delta\Psi$ depletion during the entire period of observation, suggesting that blockade of xanthine oxidase may not improve the hypoxia-induced mitochondrial dysfunction.

PGE_1 prevents zone-specific cell death during low flow hypoxia. As described elsewhere (5, 6), cell death first occurred in the midzonal regions in the midway between *P* and *C* ~ 40 min after starting low flow perfusion. Early midzonal cell death extended towards the periphery of hepatic lobules in a time-dependent manner, resulting in centrilobular necrosis. Fig. 5 shows a semiquantitative analysis of the PI-associated fluorographs. Pretreatment with BOF4272 significantly delayed the onset of the midzonal cell death and reduced the centrilobular necrosis. Pretreatment with BOF4249 had no inhibitory effect on hypoxic cell death. These data suggest that zone-specific cell death during the low flow hypoxia involves a mechanism depending on xanthine oxidase. PGE_1 treatment also attenuated zone-specific cell injury. To confirm the extracellular enzyme release as a consequence of centrilobular necrosis, the LDH activity was determined in the outlet perfusate at 120 min after the start of low flow hypoxia (Table I). The 25% low flow perfusion for 120 min induced a significant increase in the LDH levels. PGE_1 pretreatment significantly attenuated the enzyme release induced by hypoperfusion.

Prevention of hypoxia-induced paradoxical oxidative stress by PGE_1. In the hypoperfused liver, the intensity of DCF fluorescence increased, especially in the upstream regions

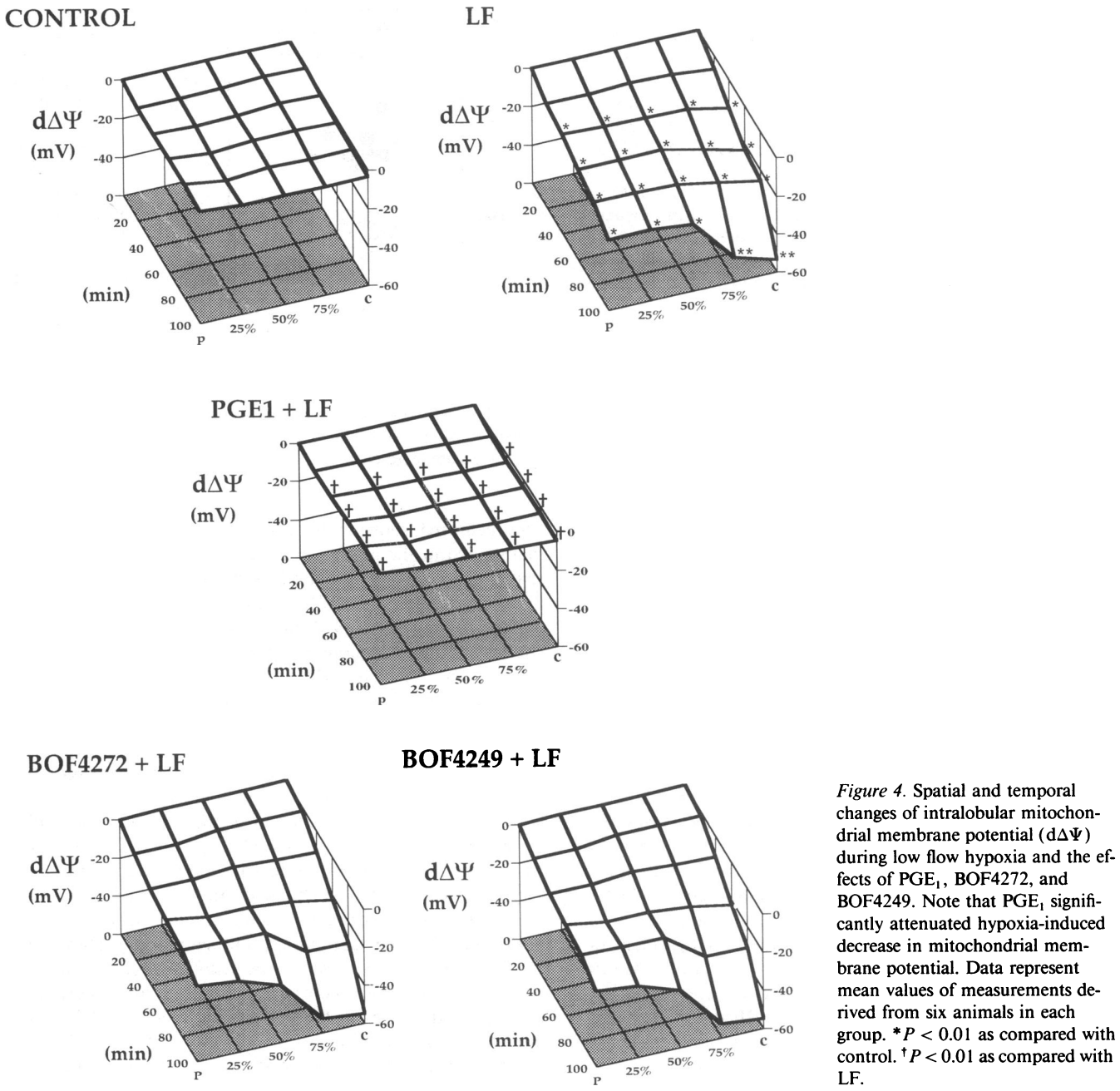

Figure 4. Spatial and temporal changes of intralobular mitochondrial membrane potential ($d\Delta\Psi$) during low flow hypoxia and the effects of PGE_1, BOF4272, and BOF4249. Note that PGE_1 significantly attenuated hypoxia-induced decrease in mitochondrial membrane potential. Data represent mean values of measurements derived from six animals in each group. $^*P < 0.01$ as compared with control. $^\dagger P < 0.01$ as compared with LF.

surrounding the periportal areas, as early as 20 min. After 40 min of low flow hypoxia, the number of multiple patchy fluorogenic sites and their fluorescence intensity increased markedly midway between the portal and the central venules and reached a maximum level after about 60 min. After reaching the maximum level, midzonal DCF fluorescence was rapidly decreased. Meanwhile, DCF fluorescence surrounding the central venules was markedly depressed without showing any significant activation during the entire course of observation (5). Fig. 6 shows the time course of midzonal DCF fluorescence in the hypoperfused liver and effects of PGE_1, BOF4272, and BOF4249. PGE_1 significantly diminished the midzonal DCF elevation. Furthermore, BOF4272, but not BOF4249, significantly attenuated early midzonal oxidative changes, suggesting that early midzonal oxidative stress is a phenomenon involving the xanthine oxidase–dependent mechanism.

Therefore, we inquired whether the attenuating effect of PGE_1 or BOF4272 on oxidative stress might be associated with their nonspecific oxyradical-scavenging properties. To clarify this possibility the effects of these reagents on an in vitro oxidant-producing system were evaluated. As shown in Fig. 7, BOF4272, but not BOF4249, significantly diminished MCLA-dependent chemiluminescence derived from the hypoxanthine–xanthine oxidase system. PGE_1 did not inhibit xanthine oxidase–dependent MCLA chemiluminescence. Furthermore, neither BOF4272 nor BOF4249 in the present concentration diminished phorbol myristate acetate–stimulated MCLA chemiluminescence yielded by a neutrophil suspension. These data suggested that PGE_1 does not scavenge superoxide anions derived from xanthine oxidase and that the antioxidant property of BOF4272 depends on its inhibitory effects on xanthine oxidase.

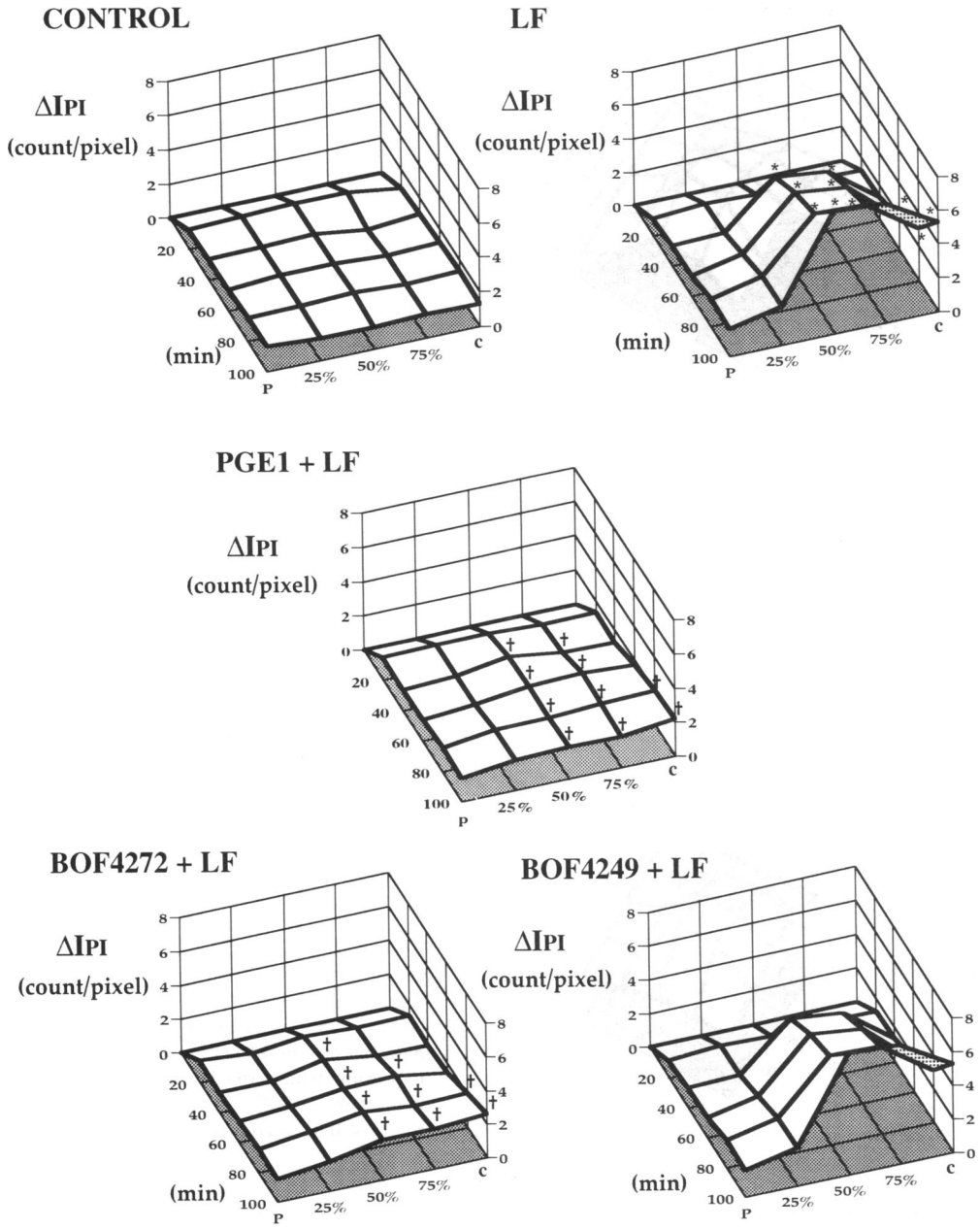

Figure 5. Spatial and temporal changes of intralobular cell damages (ΔI_{PI}) assessed by PI microfluorography and the effects of PGE_1, BOF4272, and BOF4249. The inability of BOF4249 to attenuate the hypoxia-induced cell injury suggests that the inhibitory effect of BOF4272 results from its specific inhibition of xanthine oxidase activity. Data represent mean values of measurements derived from six animals in each group. $^*P < 0.01$ as compared with control. $^\dagger P < 0.01$ as compared with LF.

Discussion

This study has demonstrated the time course and topographic distribution of reductive stress and subsequent mitochondrial dysfunction in hypoperfused liver and provides insight into the detailed mechanisms of zone-specific paradoxical oxidative injury during low flow hypoxia in the liver. According to the previous report using a microoptical fiber technique (16), in response to hypoxia, the pericentral but not periportal regions showed an increase in the pyridine nucleotide fluorescence, while both regions indicate the fluorescence increase in our method. The discrepancy seems to result from several technical problems in the previous optical fiber technique. First, the previous method did not exclude the possible contamination of vitamin A autofluorescence in Ito cells (7). Second, the pericentral fluorescence could be underestimated due to the gray density of the large pericentral venules. Finally, since a continuous ultraviolet epiillumination was used in the optical fiber method, a decrease in vitamin A autofluorescence by photobleaching would make an increase in pyridine nucleotide autofluorescence obscure in periportal regions. Our findings thus

Table I. The Release of Lactate Dehydrogenase from the Liver Exposed to 25% Low Flow Hypoxia for 120 Min

Group	Lactate dehydrogenase
	(IU per min)
Control (n = 6)	0.05±0.02
LF (n = 6)	13.5±6.2*
PGE_1 plus LF (n = 6)	0.21±0.18

* $P < 0.01$ as compared with control and the group treated with PGE_1 plus LF.

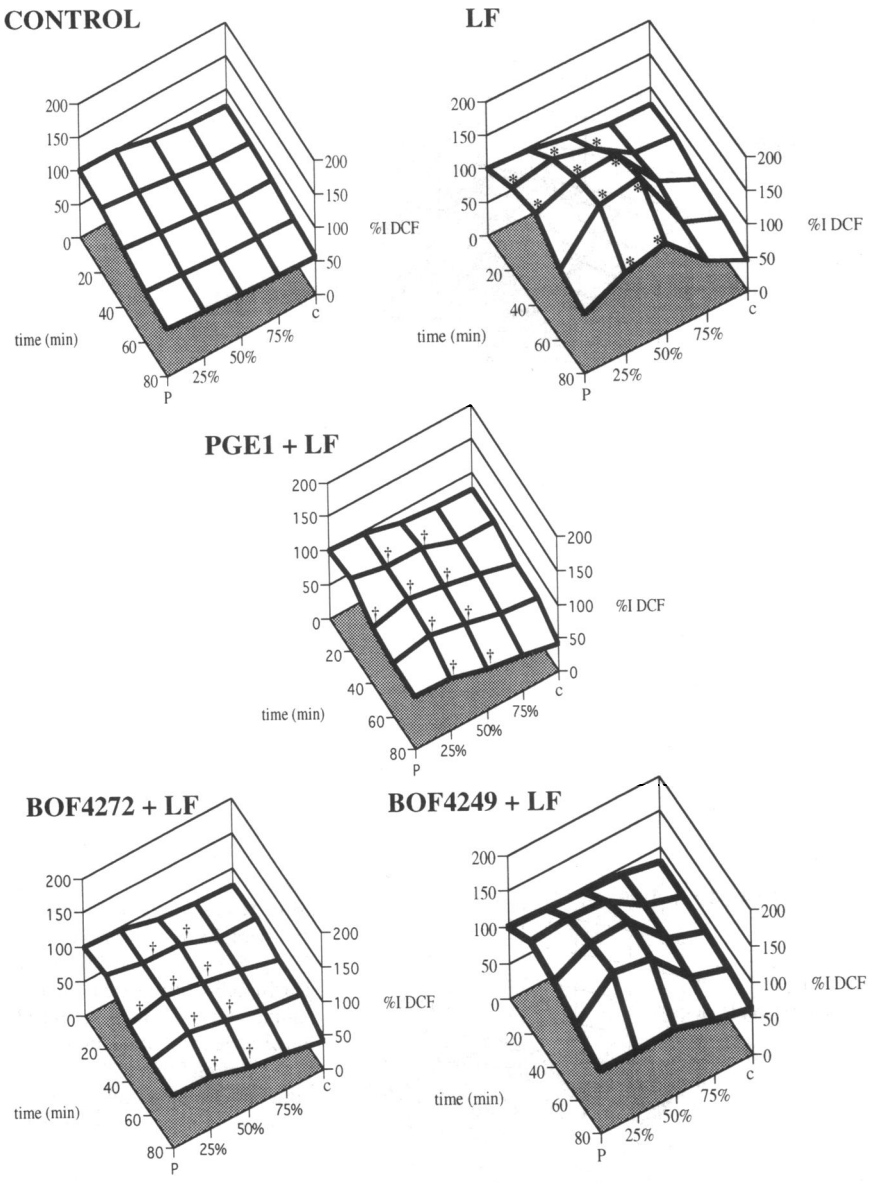

Figure 6. Effects of PGE_1 and BOF4272 on zone-specific oxidative changes $\%I_{DCF}$ induced by low flow hypoxia. BOF4249 did not attenuate the hypoxia-induced DCF increase in midzonal regions. Data represent mean values of measurements derived from six animals in each group. $^*P < 0.01$ as compared with control. $^\dagger P < 0.01$ as compared with LF.

serve as further accurate evaluation of intralobular heterogeneity in pyridine nucleotide autofluorescence in the normoperfused or hypoperfused liver.

We reported that early midzonal oxidative changes were observed as early as 20–40 min after starting the 25% low flow hypoxia and were followed by cell injury in the same regions (5, 8). Using the same experimental model, the current data show that intrahepatic saturation of NAD(P)H takes place as early as 10–20 min after starting hypoperfusion in the liver, and this early reductive change precedes a decrease in mitochondrial inner membrane potential. Intrahepatic pyridine nucleotide autofluorescence has been used as an index of impaired tissue oxygen supply and reductive changes after ultraviolet-elicited reflectance spectrophotometry became available (22). However, the pathological relevance of NADH has recently been reevaluated as a crucial factor of free radical–dependent tissue injury rather than as a mere index of tissue oxygenation.

Although we demonstrated the early midzonal hydroperoxide formation during low flow hypoxia (5), it was still unclear how the liver could be exposed to oxidative stress under relatively reductive conditions. In our previous report, pretreatment with allopurinol attenuated the zone-specific oxidative stress and subsequent centrilobular necrosis, suggesting involvement of xanthine oxidase in the oxidant-dependent cell injury mechanism. However, these findings were inconsistent with the hypothesis that the enzyme conversion from xanthine dehydrogenase to its oxyradical-producing oxidase form is a prerequisite for oxidative injury (23). Namely, since the percentage of the xanthine oxidase activity versus total oxidoreductase activity was ~ 25% during normoperfusion and showed only an additional 5% increase after 60-min hypoxic perfusion (24), the time for the enzyme conversion is too long to explain the early oxidative changes in this model. We have therefore reexamined the involvement of xanthine oxidase in the early oxidative changes by using a novel synthetic xanthine oxidase inhibitor, BOF4272. The preventive effects of this reagent on midzonal DCF elevation and subsequent PI enhancement in centrilobular regions confirmed the hypothesis that xanthine oxidase–derived oxidative stress contributes to zone-

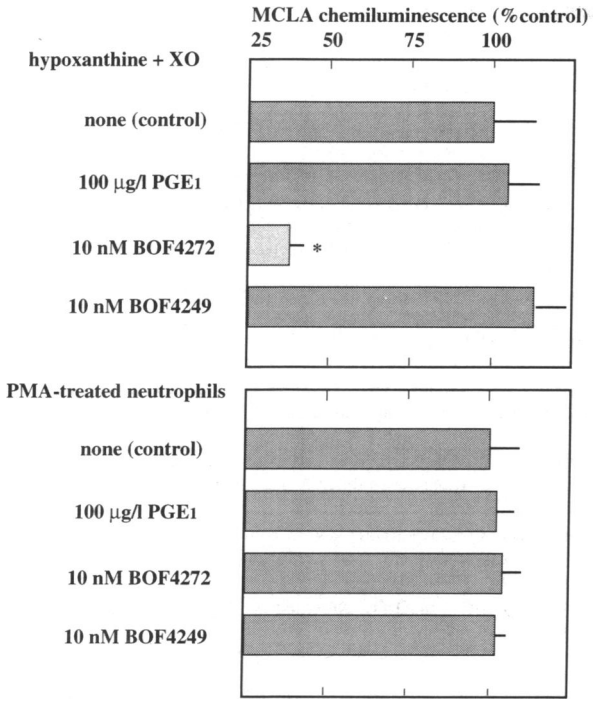

Figure 7. Effects of PGE_1 and BOF4272 on superoxide production by xanthine oxidase or neutrophils. PGE_1 attenuated neither xanthine oxidase–nor neutrophil-induced superoxide production. Note that 10 nM BOF4272, a xanthine oxidase inhibitor, showed > 60% inhibition of xanthine oxidase-induced superoxide production, whereas it did not scavenge neutrophil-elicited superoxide release. Data represent mean values of measurements derived from four separate measurements. $*P < 0.01$ as compared with control.

specific cell injury in hypoperfused liver. These results suggest the involvement of another mechanism that promotes xanthine oxidase–dependent oxidative stress independent of the enzyme conversion.

The hypoxia-induced early increase in reduced pyridine nucleotides is one such possible mechanism by which xanthine oxidase could produce profound oxidative injury during a relatively short period of hypoperfusion. The current finding clearly showed that during low flow hypoxia intrahepatic NAD(P)H saturation precedes decreasing mitochondrial inner membrane potential, midzonal hydroperoxide formation, and centrilobular cell injury. It has been reported by Nishino and Tamura (25) that NADH is a potent inhibitor of xanthine dehydrogenase but not oxidase. It is therefore quite possible that, in a reductive state where intracellular NADH is elevated enough to block the dehydrogenase activity, naturally occurring oxidase-form enzyme may catalyze hypoxanthine and oxygen to yield oxygen radicals in incompletely oxygenated midzonal regions. It also appears that NADH oxidase activity of this enzyme may serve as a possible source of superoxide production (25).

Another possibility that NAD(P)H participates in oxidative injury has recently been postulated by Jaeschke et al. (26). They showed the effects of NADH on free iron release from ferritin which enhanced hepatic microsomal lipidperoxidation induced by allyl alcohol. Since iron released from ferritin is a possible factor that propagates superoxide-dependent intracellular hydroperoxide formation via the iron-catalyzed Fenton reaction (26–28), the hypoxia-induced early NADH elevation may also facilitate iron-dependent oxidative injury in hypoperfused liver. We have recently observed that pretreatment with 2,2′-dipyridyl, a lipid-soluble iron chelator, completely abolished early midzonal DCF elevation and subsequent cell death (Suematsu et al., unpublished observation).

In this study, a novel xanthine oxidase inhibitor, BOF4272, did not inhibit early NAD(P)H elevation or subsequent mitochondrial dysfunction, whereas it did significantly diminish xanthine oxidase–dependent free radical formation and cell necrosis. These results raise the question of whether the hypoxia-induced oxidative injury could be attenuated by another new intervention that directly modulates early reductive stress per se. Our findings suggest that PGE_1 is a powerful therapeutic tool that can minimize paradoxical oxidative liver injury under hypoxic conditions. As shown by our in vitro experiments, PGE_1 is not a radical-scavenging reagent and has no inhibitory effects on xanthine oxidase. It is therefore conceivable that a protective action of PGE_1 on xanthine oxidase–mediated oxidative injury, distinct from that of allopurinol or BOF4272, may result from its preventive effects on early reductive stress and subsequent mitochondrial dysfunction. Our data suggest that this reagent may contribute to attenuation of xanthine oxidase–dependent oxidative injury, possibly by reducing NADH elevation and subsequent mitochondrial ATP degradation, which may facilitate the availability of hypoxanthine as a substrate for xanthine oxidase in incompletely oxygenated midzonal regions. PGE derivatives have been reported not only to attenuate various experimental models liver injury (29–31), but also to improve the clinical prognosis of fulminant hepatitis (32) and to prevent primary nonfunction of transplanted liver (33). However, the detailed mechanisms by which PGE_1 attenuates reductive stress and mitochondrial dysfunction in hypoxia have been quite unclear. Only a limited body of the previous experimental data showed that PGE_1 may attenuate hypoxia-induced mitochondrial dysfunction via its improving effects on blood flow in vivo (34). However, our findings showing the relationship between early reductive stress (pyridine nucleotide autofluorescence) and the corresponding sinusoidal perfusion in situ (Fig. 3) suggest that PGE_1 can improve the viability of mitochondrial function independently of its vascular actions. Further investigation is required to elucidate the mechanism through which PGE_1 attenuates reductive stress in the hypoxic liver.

Acknowledgments

The authors thank Dr. Nobuhito Goda for his technical support and suggestion, and Otsuka Pharmaceutical Factory, Inc. (Naruto, Japan) for providing BOF4272 and BOF4249. This work was supported by Grants-in-Aid for Scientific Research from the Ministry of Education, Science, and Culture of Japan, and by a grant from Keio University School of Medicine.

References

1. Lemasters, J. J., J. DiGuiseppi, A.-L. Nieminen, and B. Herman. 1987. Blebbing, free Ca^{2+} and mitochondrial membrane potential preceding cell death in hepatocytes. *Nature (Lond.)*. 325:78–81.

2. Kato, S., T. Kawase, J. Alderman, N. Inatomi, and C. S. Lieber. 1990. Role of xanthine oxidase in ethanol-induced lipid peroxidation in rats. *Gastroenterology.* 98:203–210.

3. Shaw, S. W., R. D. Gordon, S. Iwatsuki, and T. E. Starzl. 1985. Hepatic retransplantation. *Transplant. Proc.* 17:264.

4. Marotto, M. E., R. G. Thurman, and J. J. Lemasters. 1988. Early midzonal cell death during low-flow hypoxia in the isolated perfused rat liver: protection by allopurinol. *Hepatology.* 8:585–590.

5. Suematsu, M., H. Suzuki, H. Ishii, S. Kato, T. Yanagisawa, H. Asako, M. Suzuki, and M. Tsuchiya. 1992. Early midzonal oxidative stress preceding cell death in hypoperfused rat liver. *Gastroenterology.* 103:994–1001.

6. Suematsu, M., H. Suzuki, H. Ishii, S. Kato, H. Hamamatsu, S. Miura, and M. Tsuchiya. 1992. Topographic dissociation between mitochondrial dysfunction and cell death during low-flow hypoxia in perfused rat liver visualized by dual-color digital microfluorography. *Lab. Invest.* 67:434–442.

7. Suematsu, M., M. Oda, H. Suzuki, H. Kaneko, T. Furusho, S. Masushige, and M. Tsuchiya. 1993. Intravital and electron microscopic observation of Ito cells in the rat hepatic microcirculation. *Microvasc. Res.* 46:28–42.

8. Suematsu, M., H. Suzuki, H. Ishii, and M. Tsuchiya. 1993. Paradox of oxygen radical-dependent cell injury in the hypoxic liver microcirculation: with special references to intralobular functional heterogeneity. *In* Progress in Applied Microcirculation. K. Messmer, editor. S. Karger AG, Basel. 19:127–138.

9. Gores, G. J., C. E. Flarsheim, T. L. Dawson, A.-L Nieminen, B. Herman, and J. J. Lemasters. 1989. Swelling, reductive stress, and cell death during chemical hypoxia in hepatocytes. *Am. J. Physiol.* 257:C347–C354.

10. Cathcart, R., E. Schwiers, and B. Ames. 1983. Detection of picomole levels of hydroperoxides using a fluorescent dichlorofluorescein assay. *Anal. Biochem.* 134:111–116.

11. Suematsu, M., S. Kato, H. Ishii, H. Asako, T. Yanagisawa, H. Suzuki, C. Oshio, and M. Tsuchiya. 1991. Intralobular heterogeneity of carbon tetrachloride-induced oxidative stress visualized by digital imaging fluorescence microscopy. *Lab. Invest.* 64:167–173.

12. Emanus, R. K., R. Grunwald, and J. J. Lemasters. 1986. Rhodamine 123 as a probe of transmembrane potential in isolated rat liver mitochondria: spectral and metabolic properties. *Biochim. Biophys. Acta.* 850:436–448.

13. Suematsu, M., C. Oshio, S. Miura, and M. Tsuchiya. 1987. Real-time visualization of oxyradical burst from single neutrophil by using ultrasensitive video intensifier microscopy. *Biochem. Biophys. Res. Commun.* 149:1106–1110.

14. Suematsu, M., I. Kurose, H. Asako, S. Miura, and M. Tsuchiya. 1989. In vivo visualization of oxyradical-dependent photoemission during endothelium-granulocyte interaction in microvascular beds treated with platelet-activating factor. *J. Biochem.* 106:355–360.

15. Herman, B., A.-L. Nieminen, G. J. Gores, and J. J. Lemasters. 1989. Blebbing, cytosolic free calcium, and mitochondrial membrane potential following toxic and anoxic injury in hepatocytes. *In* Integration of Mitochondrial Function. J. J. Lemasters, C. R. Hackenbrock, and R. G. Thurman, editors. Plenum Publishing Corp., New York. 379 pp.

16. Lemasters, J. J., S. Ji, and R. G. Thurman. 1981. Centrilobular injury following hypoxia in isolated perfused rat liver. *Science (Wash. DC).* 213:661–663.

17. Suzuki, H., M. Suematsu, H. Ishii, S. Kato, Y. Horie, M. Mori, S. Miura, and M. Tsuchiya. 1992. Zonal heterogeneity of redox state and its topographic correlation with xanthine oxidase-mediated oxidative stress in hypoperfused rat liver. *Hepatology.* 16:158*a*. (Abstr.)

18. Sato, S., K. Tatsumi, and T. Nishino. 1991. A novel xanthine dehydrogenase inhibitor, BOF-4272. *Adv. Exp. Med. Biol.* 309A:135–138.

19. Nakano, M. 1990. Determination of superoxide radical and singlet oxygen based on chemiluminescence of luciferin analogs. *Methods Enzymol.* 186:585–591.

20. Shimmura, S., K. Tsubota, Y. Oguchi, D. Fukumura, M. Suematsu, and M. Tsuchiya. 1992. Oxyradical-dependent photoemission induced by a phacoemulsification probe. *Invest. Ophthalmol. & Visual Sci.* 33:2904–2907.

21. Suematsu, M., M. Suzuki, T. Kitahora, S. Miura, K. Suzuki, T. Hibi, M. Watanabe, H. Nagata, H. Asakura, and M. Tsuchiya. 1987. Increased respiratory burst of leukocytes in inflammatory bowel diseases. The analysis of free radical generation by using chemiluminescence probe. *J. Clin. Lab. Immunol.* 24:125–128.

22. Quistorff, B., B. Chance, and H. Takeda. 1978. Two- and three-dimensional redox heterogeneity of rat liver. Effects of anoxia and alcohol on the lobular redox pattern. *In* Frontiers of Biological Energetics. Vol 2. Academic Press, New York. 1487–1497.

23. Roy, R. S., and J. M. McCord. 1983. Superoxide and ischemia: conversion of xanthine dehydrogenase to xanthine oxidase. *In* Oxy Radicals and Their Scavenger Systems. II. Cellular and Medical Aspects. R. A. Greenwald and G. Cohen, editors. Elsevier Science Publishing Co. Inc., New York. 145–153.

24. Brass, C. A., J. Narciso, and J. L. Gollan. 1991. Enhanced activity of the free radical producing enzyme xanthine oxidase in hypoxic rat liver. Regulation and pathophysiologic significance. *J. Clin. Invest.* 87:424–431.

25. Nishino, T., and I. Tamura. 1991. The mechanism of conversion of xanthine dehydrogenase and the role of the enzyme in reperfusion injury. *Adv. Exp. Med. Biol.* 309A:327–333.

26. Jaeschke, H., C. Kleinwaechter, and A. Wendel. 1992. NADH-dependent reductive stress and ferritin-bound iron in allyl alcohol-induced lipid peroxidation in vivo: the protective effect of vitamin E. *Chem. Biol. Interact.* 81:57–68.

27. Gutteridge, J. M. C., L. Maidt, and L. Poyer. 1990. Superoxide dismutase and Fenton chemistry. *Biochem. J.* 269:169–174.

28. Suematsu, M., G. W. Schmid-Schönbein, R. H. Chavez-Chavez, T. T. Yee, T. Tamatani, M. Miyasaka, F. A. DeLano, and B. W. Zweifach. 1993. In vivo visualization of oxidative changes in microvessels during neutrophil activation. *Am. J. Physiol. (Heart & Circ. Physiol.).* 264:881–891.

29. Abecassis, M., J. A. Falk, L. Makowka, V. J. Dindzans, R. E. Falk, and G. A. Levy. 1987. 16,16 Dimethyl prostaglandin E_2 prevents the development of fluminant hepatitis and blocks the induction of monocyte/macrophage procoagulant activity after murine hepatitis virus strain 3 infection. *J. Clin. Invest.* 80:881–889.

30. Stachura, J., A. Tarnawski, K. J. Ivey, T. Mach, J. Bogdal, J. Szczudrasia, and B. Klimczyk. 1981. Prostaglandin protection of carbon tetrachloride-induced liver cell necrosis in the rat. *Gastroenterology.* 81:211–217.

31. Mizoguchi, Y., H. Tsutsui, and K. Miyajima. 1987. The protective effects of prostaglandin E_1 in an experimental massive hepatic cell necrosis model. *Hepatology.* 7:1184–1188.

32. Levy, G. 1987. Treatment of fluminant hepatitis with continuous infusion of prostin VR (PGE_1). *Hepatology.* 7:1104*a*. (Abstr.)

33. Greig, P. D., G. M. Woolf, S. B. Sinclair, M. Abecassis, S. M. Strasberg, B. R. Taylor, L. M. Blendis, R. A. Superina, M. F. X. Glynn, B. Langer et al. 1989. Treatment of primary liver graft nonfunction with prostaglandin E_1. *Transplantation (Baltimore).* 48:447–453.

34. Kurokawa, T., T. Nonami, A. Harada, A. Nakao, S. Sugiyama, T. Ozawa, and H. Takagi. 1991. Effects of prostaglandin E_1 on the recovery of ischemia-induced liver mitochondrial dysfunction in rats with cirrhosis. *Scand. J. Gastroenterol.* 26:269–274.